Energies **2014**, *7*, 6118-6141; doi:10.3390/en7096118

OPEN ACCESS

energies

ISSN 1996-1073

www.mdpi.com/journal/energies

Article

Methane Flux and Authigenic Carbonate in Shallow Sediments Overlying Methane Hydrate Bearing Strata in Alaminos Canyon, Gulf of Mexico

Joseph P. Smith [1,*] and Richard B. Coffin [2,†]

[1] Oceanography Department, U.S. Naval Academy, 572C Holloway Road, Annapolis, MD 21402, USA

[2] Marine Biogeochemistry (Code 6114), U.S. Naval Research Laboratory, Washington, DC 20375, USA; E-Mail: richard.coffin@tamucc.edu

[†] Current Address: Department of Physical and Environment Sciences, Texas A&M University-Corpus Christi, Corpus Christi, TX 78412, USA.

[*] Author to whom correspondence should be addressed; E-Mail: jpsmith@usna.edu; Tel.: +1-410-293-6568; Fax: +1-410-293-2137.

Received: 11 August 2014; in revised form: 4 September 2014 / Accepted: 9 September 2014 / Published: 23 September 2014

Abstract: In June 2007 sediment cores were collected in Alaminos Canyon, Gulf of Mexico across a series of seismic data profiles indicating rapid transitions between the presence of methane hydrates and vertical gas flux. Vertical profiles of dissolved sulfate, chloride, calcium, magnesium, and dissolved inorganic carbon (DIC) concentrations in porewaters, headspace methane, and solid phase carbonate concentrations were measured at each core location to investigate the cycling of methane-derived carbon in shallow sediments overlying the hydrate bearing strata. When integrated with stable carbon isotope ratios of DIC, geochemical results suggest a significant fraction of the methane flux at this site is cycled into the inorganic carbon pool. The incorporation of methane-derived carbon into dissolved and solid inorganic carbon phases represents a significant sink in local carbon cycling and plays a role in regulating the flux of methane to the overlying water column at Alaminos Canyon. Targeted, high-resolution geochemical characterization of the biogeochemical cycling of methane-derived carbon in shallow sediments overlying hydrate bearing strata like those in Alaminos Canyon is critical to quantifying methane flux and estimating methane hydrate distributions in gas hydrate bearing marine sediments.

Keywords: methane; hydrate; Gulf of Mexico; Alaminos Canyon; sediments; porewaters; carbon cycling

1. Introduction

Natural gas hydrates are crystalline clathrate compounds consisting of hydrocarbon guest molecules such as methane (CH_4) within a solid water lattice. The largest accumulations of natural gas hydrates occur in offshore and continental (active and passive) margin sediments and, to a lesser extent, in permafrost, where high pressure, low temperatures, and methane concentrations present in excess of solubility promote the formation and stability of solid phase clathrates. Methane hydrates constitute a major organic carbon sink and a vast potential energy source [1]. Methane hydrates are also important to global climate and coastal slope stability.

Substantial research has focused on carbon cycling in hydrate bearing sediments. The presence of shallow gas hydrates is normally inferred through geochemical [2,3] and geophysical [4] data interpretation as well as the existence of unique biological communities [5,6]. No one line of evidence has proven to be a unique indicator of the presence of shallow gas hydrates [7–9].

Authigenic carbonates have been shown to occur in sediments containing CH_4 hydrates and in sediments at or near the seafloor over CH_4 hydrate deposits [10–21]. Carbonate structures and concretions can form on the seafloor in areas with a significant CH_4 flux [11,14,16,21], carbonate horizons can be formed in the sediments as a result of microbially-mediated oxidation of CH_4 [13,19], and authigenic carbonates are often associated with faults that act as conduits for the upward migration of fluids and CH_4 [10]. Carbonate is an essential base for establishing benthic communities supported by the biogeochemical cycling of CH_4 in sediments and bottom waters at cold seeps and CH_4 hydrate deposits [6]. Carbonate in hydrate bearing sediments can be biogenic and/or authigenic carbonate derived from dissolved inorganic carbon (DIC) in seawater or from DIC generated during the oxidation of organic matter, methane, or non-methane hydrocarbons [17]. Variations in the composition of carbonate minerals in the sediments can be due to past changes in the stability limits of gas-hydrate host deposits and can provide a past record of CH_4 hydrate destabilization [10–13,16,20,21].

There exists a close relationship between gas hydrates, CH_4 flux, the oxidation of organic matter through sulfate reduction (SR), the anaerobic oxidation of methane (AOM), and authigenic carbonate mineralization in marine sediments containing or overlying CH_4 hydrate. High concentrations of authigenic carbonate do potentially indicate elevated rates of AOM, and can provide a record of such processes [12,13,16–18,21]. The precipitation of authigenic minerals (aragonite, Mg-calcite, dolomite) in such areas represents a potentially significant carbon sink and plays a role in regulating the flux of methane to the overlying water column and atmosphere [22].

In cold-seep and gas-hydrate influenced sediments, authigenic minerals (aragonite, Mg-calcite, dolomite) can precipitate from the oxidation of methane-rich fluids. Carbonate precipitates as a secondary reaction of the oxidation of organic matter by sulfate reduction (SR) and/or AOM. The net reactions for SR and AOM are:

$$2(CH_2O)_n + SO_4^{2-} \rightarrow 2HCO_3^- + H_2S \quad \text{Sulfate Reduction (SR)} \quad (1)$$

$$CH_4 + SO_4^{2-} \rightarrow HCO_3^- + HS^- + H_2O \quad \text{Anaerobic Oxidation of Methane (AOM)} \quad (2)$$

Whereas aerobic oxidation promotes the dissolution of carbonate in surficial sediments through the lowering of porewater pH, the coupled effect of the microbially-mediated diagenetic reactions shown above, SR and AOM, increase porewater alkalinity (generate bicarbonate). In the presence of seawater-derived cations (Ca^{2+}, Mg^{2+}) this can lead to precipitation of authigenic carbonates [23–25], shown by the net reaction below:

$$Ca^{2+} + HCO_3^- \rightarrow H^+ + CaCO_3\ (s) \quad (3)$$

In sediments overlying suspected hydrate deposits, high concentrations of authigenic carbonate can indicate elevated rates of AOM. Precipitation can occur at or around the sulfate-methane interface (SMI) or through a sulfate methane transition (SMT). The SMT is a border between sulfate-bearing sediment above and sulfate-depleted, methane-rich sediments below. The SMT is a zone of intense methane oxidation [2,24]. Carbonate precipitation associated with methane oxidation commonly forms discrete mm size concretions in hydrate bearing sediments [20,26].

Temperature, the level of porewater saturation of HCO_3^- and cations such as Ca^{2+} and Mg^{2+}, and sediment redox state are major factors influencing the precipitation of different carbonate minerals. Physical and chemical characteristics of sediments containing hydrates provide distinct diagenetic environments that can promote precipitation and preservation of carbonate minerals. Chemical controls on the formation of specific carbonate species are difficult to evaluate [13,27]. Because of this difficulty and the fact that gas hydrates are not generally preserved in conventional core samples, it is necessary to find diagenetic proxies to quantify biogeochemical processes and identify sediments that formerly contained gas hydrate.

Although the interstitial environment controls specific carbonate diagenetic processes, carbonate dissolution or precipitation will produce notable changes in sediment porewater profiles of Ca^{2+}, Mg^{2+}, and Sr^{2+} [13,16,20–24]. Porewaters modified by carbonate diagenesis may be characterized by the direction and gradient of the ratios of these constituents [13,20,21,23,26]. Steep vertical and horizontal gradients of Ca^{2+}, Mg^{2+}, and Sr^{2+} can develop on fine scales (centimeters to decimeters) in porewater and sediment of methane bearing strata as a secondary consequence of diffusion, fluid advection, methane supply, and AOM [13,20,21,23,26]. Precipitates of authigenic minerals mark areas of fluid flow, and are the result of biogeochemical processes and interaction (mixing) of porewater fluids and ambient seawater [12]. Authigenic carbonates can provide and integrated record of such processes [17].

Directly measuring methane fluxes in sediment porewaters is problematic since samples recovered from depth depressurize quickly leading to a change in the partial pressure for methane gas solubility in seawater. Porewater headspace CH_4 measurements on samples collected from depressurized sediments, however, do provide at least a relative assessment of spatial variation in methane concentrations. Other biogeochemical indicators exist to aid in quantification and qualification of methane fluxes and methane-derived carbon cycling between organic and inorganic phases in sediments overlying hydrate bearing strata.

Destabilization of gas hydrates leads to a freshening of porewaters that can be seen in Cl^- profiles [28]. Seawater contains large amounts of sulfate (SO_4^{2-}), which diffuses downward into pore waters and

contributes to diagenesis [2]. Under anoxic conditions, SO_4^{2-} depletes as depth increases in sediment due to organoclastic SR of organic matter by microbial activity. Sulfate can also be reduced through AOM. If AOM is the dominant process consuming SO_4^{2-}, usually due to high methane concentrations deeper in the sediments, SO_4^{2-} diffusion into the sediments is inversely related to upward CH_4 flux with a 1:1 stoichiometry. Assuming steady-state conditions, the slope of sediment porewater SO_4^{2-} concentration profiles can therefore be used to interpret upward CH_4 flux from below. Nonlinearity in the slope of sediment porewater SO_4^{2-} concentration profiles could result from sulfate consumption due to sulfate reduction, sulfate gradient instability, fluid advection, bioturbation, and input of organic matter from sedimentation [3].

The stable carbon isotope ratio, or ratio of stable heavy carbon (^{13}C) to light carbon (^{12}C) of dissolved or gaseous methane ($\delta^{13}C$-CH_4), in porewaters can be used to distinguish between biogenic and thermogenic sources. Dissolved inorganic carbon (DIC) profiles and $\delta^{13}C$-DIC values will also lend information on methane flux and AOM rates [20–24,29]. Carbonates formed as a secondary consequence of AOM will have a distinct $\delta^{13}C$ signature indicative of the parent carbon source.

Dissolved inorganic carbon is the sum of all dissolved inorganic carbon species and is dominated by bicarbonate and carbonate (HCO_3^- and CO_3^{2-}), which both contribute to alkalinity. Comparing alkalinity profiles to the sulfate profiles may help determine if SR or AOM dominates the sulfate depletion process in shallow sediment porewaters. Microbial and thermogenic methane production contribute to the DIC concentration in the form of HCO_3^- [20]. Calcium (Ca^{2+}) and Mg^{2+} both chemically precipitate HCO_3^- in the form of marine carbonates. Therefore, the net DIC flux can be calculated by subtracting the Ca^{2+} and Mg^{2+} flux from the DIC flux estimated from measured porewater concentration values [20,21,29].

If AOM dominates, the net DIC flux should compare to the sulfate flux with a 1:1 ratio above the SMT. If SR dominates, the ratio will approach 2:1. Dissolved inorganic carbon concentrations and $\delta^{13}C$ may also be used to evaluate area of active methane oxidation release since they alter in response to the presence of methane [30]. However, DIC levels are not an absolute confirmation of methane oxidation as increases in bicarbonate can also result from fermentation, or reduction of solid organic matter. A decrease may be attributed to the mineralization of authigenic carbonate [20]. Integration of geochemical measurements in sediments and interstitial porewater fluids allows for resolution of the interaction between fluid flow and microbially-mediated diagenic processes in the cycling of methane-derived carbon in shallow sediments overlying methane hydrate bearing strata [20,21,29].

The Gulf of Mexico (GoM) contains both microbial and thermogenic methane hydrates, distinguishable through their carbon isotopic composition ($\delta^{13}C$-CH_4) [31]. Originating from below the bottom of the gas hydrate stability zone (GHSZ), thermogenic methane migrates upward via channels and faults until it can combine with water to become hydrate. The nature of thermogenic methane formation allows for more localized distribution, maturity, and accumulation in massive amounts [32]. Because of the presence of fault associated conduits in the GoM thermogenic methane hydrate is common, especially in localized areas [28]. Biogenic methane is formed at much shallower depths in sediments through the oxidation of organic matter by bacteria under anoxic conditions both below and within and above the GHSZ. Biogenic methane hydrate deposits are also common in certain areas of the GoM but tend to be less localized and occur at lower concentrations [28,32]. Coupling geophysical and geochemical data from shallow sediment to infer methane flux is a method that can be employed to help interpret the location, source, and quantity of methane hydrate reservoirs for potential energy use and

climate impact analysis [3]. In June 2007, a targeted transect of shallow sediment cores was collected from the seafloor of the Alaminos Canyon region of the GoM in an area where previous seismic surveys indicated rapid transitions between the presence of methane hydrates and vertical gas flux. Geochemical characterization of sediments and porewaters collected were used to show that a significant fraction of the vertical methane flux is cycled into inorganic carbon and that incorporation of methane-derived carbon into dissolved and solid inorganic carbon phases represents a significant carbon sink regulating the flux of methane to the overlying water column and atmosphere at Alaminos Canyon and potentially other site with gas hydrate bearing marine sediments.

2. Methods

2.1. Study Area

The Alaminos Canyon (AC) is a deep water canyon (~1000–3000 m) located in the northwestern Gulf of Mexico (Figure 1). The geology of the area is dominated by northeast-southwest trending salt-cored box folds of the Perdido fold belt which lie beneath a thick, mobile salt canopy [33,34]. Research by others has identified Block 818 in AC as a site of significant hydrocarbon flux and oil, gas, and gas hydrate accumulation [33–39] in a variety of turbidite deposits from sand sheets to amalgamated and leveed channel systems [36]. Boswell *et al.* [34] used well data and 3-D seismic data to show evidence for significant, concentrated gas hydrate accumulation near the AC 818 #1 ("Tigershark") well. Uplift of the Perdido fold belt has raised gas reservoirs in Oligocene Frio sands within the Lower Tertiary deepwater turbidite to shallow depths above the base of the gas hydrate stability (BGHS) zone. The Oligocene Frio sand is very fine-grained, immature volcaniclastic sand with a high porosity [34].

In June 2007, the Gulf of Mexico Gas Hydrate Joint Industry Project (JIP) teamed with the U.S. Naval Research Laboratory (NRL) and the Seep and Methane Hydrate Advanced Research Initiative to conduct fieldwork in AC Block 818 [39]. The goal of the NRL-led AC-07 research expedition was to interpret seismic profiles and collect geochemical data to conduct preliminary site characterization of deep sediment hydrate deposits within the region for use in JIP deep drilling efforts. Field sampling and data collection locations for the AC-07 research expedition were based on seismic profiles provide by WesternGeco and reviewed by geophysists and geochemists from WesternGeco, NRL, the U.S. Department of Energy, National Energy Technology Laboratory (NETL) and the U.S. Mineral Management Service (MMS). Seismic reflection maps (WesternGeco) display subtle differences in reflection amplitude created by high levels of sand layering below a 10 m thick pelagic drape and show a focused location of vertical gas migration near an existing well. The seeps are located along a small ridge associated with the up-thrown side of a fault. No gas chimneys are visible in 3-D seismic data. Well data suggests a thick 5 to 50 m of hydrate laden, sandy sediment [39].

Figure 1. Map showing the location of Alaminos Canyon (AC) in the Gulf of Mexico (GoM). Inlet shows detail of survey block AC 818 containing seismic line 986 (dashed line). Black dots indicate locations of piston cores collected by the U.S. Naval Research Laboratory (NRL) as part of the AC-07 methane hydrate research expedition, June 2007 (Map modified from Google Earth using data from U.S. Geological Survey (USGS), National Archive of Marine Seismic Surveys; Texas A&M University, Gulf of Mexico Coastal Ocean Observing System (GCOOS), Coastal Relief Model for the Gulf of Mexico; and WesternGeco).

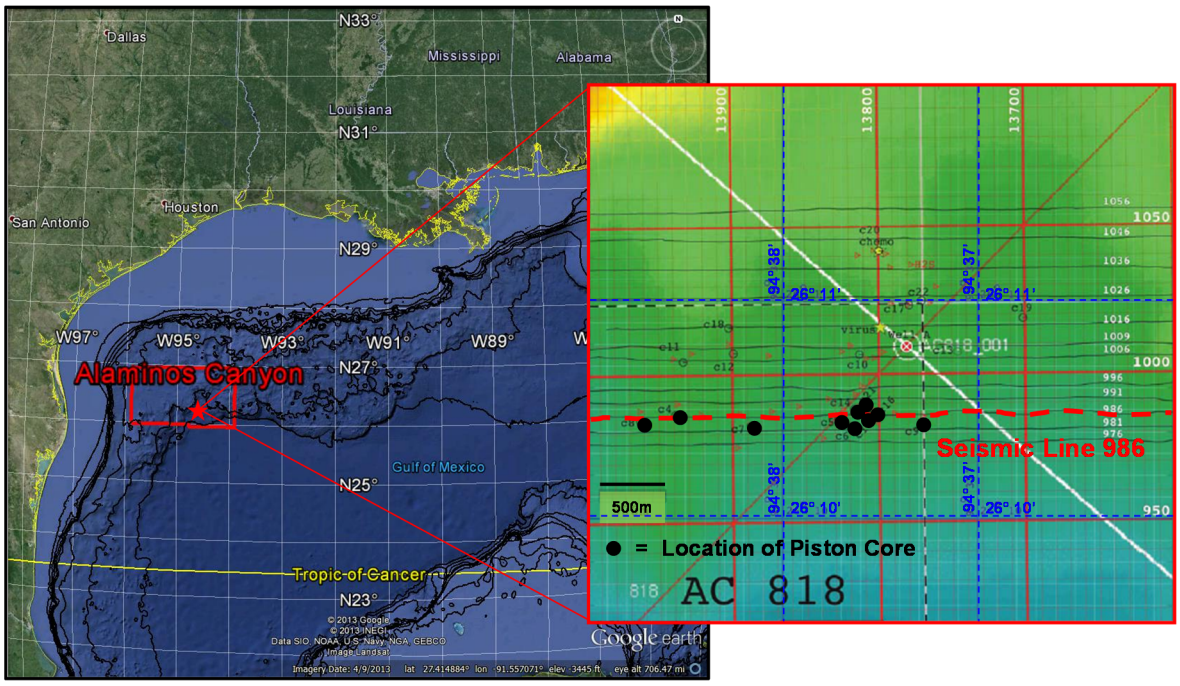

2.2. Sample Collection

In June 2007, a series of 10 piston cores (PC-04, PC-05, PC-06, PC-07, PC-08, PC-08, PC-14, PC-15, PC-16, PC-21) were collected from R/V *Cape Hatteras* along WesternGeco inline 986 in AC Block 818 (Figure 2) Seismic data on inline 986 revealed an area of potential gas hydrate accumulation overlying free gas accumulation marked by prominent bottom simulating reflectors (BSRs). The seismic data also suggested possible gas venting through a small seep feature on the seafloor. Piston cores were collected along a roughly 3 km linear transect across the suspected seep feature [39].

Sediment cores were processed using the methods detailed in Coffin *et al.* [3,39]. The sediment cores were collected using a 10 m piston coring system (Milbar Hydro-Test, Inc., Shreveport, LA, USA) that consisted of 2-3 N-80 alloy core barrels lined with 7 cm outer diameter polycarbonate barrels connected by a modified Atlas Bradford connections system. The core weight used was approximately 1400 kg. Trigger weights were set initially at 12–15 m. Typical core penetration depths were between 3 m and 8 m. An NRL Sonardyne Ultra-Short BaseLine (USBL) positioning and tracking system attached 50 m above the core head was used to provide acoustic positioning on all but one piston core deployments. This instrument provided improved accuracy in positioning but deep currents were still responsible for drifts of up to 130 m from the ship's position on the surface. The ship was able to maneuver within a range of 10–40 m from the acoustic positioning.

Figure 2. Locations for piston cores collected during the AC-07 research expedition along the WesternGeco seismic profile for Inline 986. The seismic profile has been colorized to indicate areas of potential hydrate deposits located above interpretation of free gas zones and free gas venting.

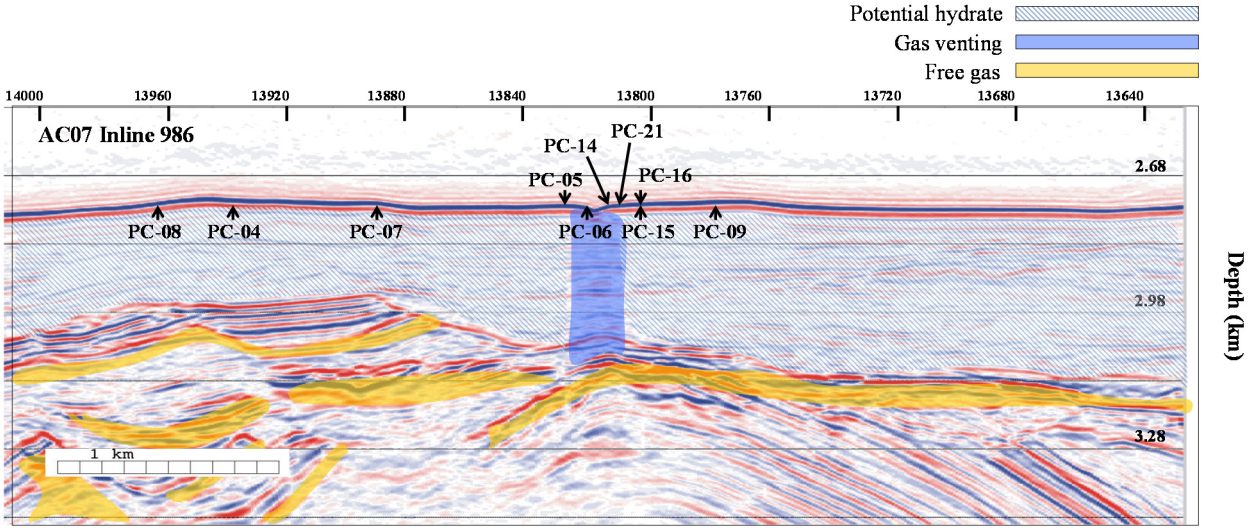

2.3. Sample Processing

Immediately after retrieval, core liners were removed, placed horizontally on deck, and inspected for gas pockets and gas expansion voids. At void spaces, the liner was drilled and gas sampled with a 60 mL polypropylene syringe fitted with a modified 3-way stopcock. Gas samples were then transferred to 30 mL pre-evacuated, glass serum vials fitted with a gastight stopper and aluminum seal for subsequent analysis to determine relative light hydrocarbon concentrations and isotopic ratios. Cores were cut in 10 cm round sections at 25 to 45 cm intervals. The sampling interval was adjusted based upon observations of dark (black) sediment and hydrogen sulfide odor and the appearance of core gas pockets. On average, 20 sediment sections were sampled from each core.

Sediment plugs were immediately collected from each core round after sectioning using a 3 mL polypropylene syringe with the tip cut off. Sediment plugs were transferred to pre-weighed 20 mL serum vials and capped with gastight stoppers and aluminum seals to determine sediment headspace light hydrocarbon concentrations (CH_4 through C_3H_8) [40] as well as $\delta^{13}C_{CH4(g)}$ ratios. Whole round core sections were then taken to the ship wet laboratory for processing.

Approximately 5 g of wet sediment was collected from each whole round section using a clean Al spatula and transferred into pre-weighed 31-mm snap-tight Petri-dishes. These sub-samples were frozen for use in laboratory measurements of sediment porosity and percent organic carbon. Immediately after the subsample collection, porewater was pressed from the remaining sediment from each round using Reeburgh-style PVC press containers pressurized to ~400 KPa (~60 psi) by low-pressure air applied to a latex sheet placed between the core sections and press gas inflow. Porewater was pre-filtered through Grade 1 Qualitative Filter Paper into gas-tight 60-mL polypropylene syringes and then again through 0.2-µm Acrodisc PES syringe filters (Pall) into ashed (4 h at 450 °C) 20 mL vials. Waters were then further distributed into 1–10 vials for each subsequent analysis and chemically fixed, if necessary to stop microbial activity [3,39]. The remaining pressed sediment was wrapped in ashed aluminum foil, sealed

in Whirlpack bags, stored frozen at −20 °C, and transported to the land-based laboratory for inorganic and organic carbon concentration and isotope analyses.

2.4. Sample and Data Analysis

Headspace methane (CH_4) and porewater sulfate (SO_4^{2-}) and chloride (Cl^-) concentrations were determined onboard ship. Analyses of porewater dissolved inorganic carbon (DIC) concentrations, stable carbon isotope ratios (δ^{13}C-DIC), and major cation concentrations (Ca^{2+}, Mg^{2+}) were conducted at the NRL laboratory as was solid phase analysis for sediment porosity and carbonate content ($CaCO_3$).

Volumetric CH_4 gas concentrations were determined from the 3 mL sediment plugs using headspace techniques and were quantified against certified gas standards (Scott Gas) [40]. Analysis was performed using a Shimadzu 14-A gas chromatograph (GC, Kyoto, Japan) equipped with a flame ionization detector and Hayesep-Q 80/100 column. Gases were separated isothermally at 50 °C. Final relative concentrations were calculated using sediment porosity and dry weight data obtained at the U.S. Naval Research Laboratory [40]. True CH_4 concentrations cannot be reliably measured from porewater samples because pressure reduction during core recovery lowers solubility and transfers dissolved CH_4 to the gas phase. Hence, headspace CH_4 data presented are used only to provide data comparisons with measured SO_4^{2-} gradients.

Sulfate and Cl^- concentrations were measured with a Thermo-Fisher Dionex DX-120 ion chromatograph (Sunnyvale, CA, USA) equipped with an AS-9HC column, Anion Self-Regenerating Suppressor (ASRS Ultra II), and an AS-40 autosampler [28]. Samples were diluted 1:50 (vol/vol) and measured against diluted IAPSO standard seawater (28.9 mM SO_4^{2-}, 559 mM Cl^-). Analytical precision was ±1% of the standards.

Major cation concentrations (Ca^{2+}, Mg^{2+}) in sediment porewaters were also measured using a Thermo-Fisher Dionex DX-120 ion chromatograph equipped with an AS-40 autosampler in the laboratory. A 20 mM methanesulfonic acid (CH_3SO_2OH) eluent was used with a CS-12 column and a Cation Self-Regenerating Suppressor (CSRS Ultra II) at a flow rate of ~0.7 mL/min. Samples again were diluted 1:50 (vol/vol). Calibration standards were prepared in the laboratory and diluted (1:50) IAPSO standard seawater was used as a reference standard. Analytical precision was ±2%–3%.

Porewater DIC concentrations were measured using a UIC CO_2 coulometer and standardized to a certified seawater reference material (University of California, San Diego, CA, USA). The conversion of DIC to CO_2 and separation from interfering sulfides was conducted according to Boehme *et al.* [41].

Sediment total carbon and OC (%TC, %SOC) concentrations and δ^{13}C values were determined on a Fisons EA 1108 C/H/N analyzer in line with a Thermo Electron Delta Plus XP Isotope Ratio Mass Spectrometer (IRMS) interface via a Conflo II. Pressed sediment was dried at 80 °C, ground with a mortar and pestle, then 15 to 20 mg of sediment was weighed in tin capsules for TC analysis. For SOC analysis, sub-samples were weighed in silver capsules, treated with an excess of 10% HCl and dried in an oven at 70 °C overnight to remove inorganic carbon. A concentration calibration curve for carbon concentration analysis was generated daily by analyzing and acetanilide standard. Sediment carbonate concentrations (%$CaCO_3$) concentrations were estimated by multiplying the difference between %TC and %SOC by the ratio of the molar mass of $CaCO_3$ to carbon, assuming calcite and aragonite as the dominant carbonates:

$$\%CaCO_3 = (\%TC - \%SOC) \times 8.33 \quad (4)$$

Pore water dissolved inorganic carbon $\delta^{13}C$ ratios ($\delta^{13}C$-DIC) and gas pocket and sediment $\delta^{13}C$-CH_4 ratios were determined using a Thermo Electron Trace GC (Waltham, MA, USA) equipped with a Varian Porapak-Q column and GC-CIII combustion interface in-line with a Delta Plus XP IRMS [3,42,43]. For $\delta^{13}C$-DIC analysis, 2 mL porewater samples were treated with 200 µL of 85% H_3PO_4. The CO_2 was extracted from the vial headspace and injected into the GC via a split/splitless inlet in split mode. All $\delta^{13}C$-DIC values were normalized through analysis of CO_2 and C_1-C_5 alkanes in NIST RM 8560 (natural gas, petroleum origin). Samples for $\delta^{13}C$-CH_4 analysis were introduced via an in-line cryogenic focusing system according to the method of Plummer *et al.* [42]. A separate $\delta^{13}C$ normalization curve was generated for C_1-C_4 alkanes and used to normalize $\delta^{13}C$-CH_4 data. Replicate $\delta^{13}C$-DIC values varied by less than 0.5‰, and $\delta^{13}C$-CH_4 by less than 1.0‰ [40]. Stable carbon isotope ratios are presented in per mil units compared to a PeeDee Belmenite standard.

Sediment porosity was estimated using the method described by Hoehler *et al.* [40]. Frozen samples (~5–6 g) were thawed and allowed to equilibrate to room temperature. Samples were weighed wet and placed in a drying oven (~50–60 °C) for 24–48 h. Samples were then weighed again after drying. Sediment water content was determined by the difference between wet and dry weight, assuming constant pore water (ρ_{pw}) and bottom water (ρ_{sw}) density. Porosity (φ) was then determined using the following equation:

$$\text{Porosity } (\varphi) = \rho_{sm}WC \times [1/(\rho_{sm}WC + \rho_{pw}(1 - WC)] \quad (5)$$

where: assumed solid matter density (ρ_{sm}) = 2.50 g/cm^3.

3. Results

3.1. Sediment Headspace CH_4 and Porewater SO_4^{2-} and Cl^- Concentrations

Figure 3 shows measured sediment headspace CH_4 and porewater SO_4^{2-} and Cl^- concentrations *vs.* depth for the AC-07 piston cores. With the exception of core PC-06, measured porewater Cl^- concentrations were consistently near seawater values (559 mM) in all piston cores. The Cl^- profile in PC-06 clearly shows a freshening of porewaters due to the destabilization of solid phase hydrates during core collection. Consequently, measured headspace CH_4 values in PC-06 ranged from 1.5 to 18.9 mM throughout the entire length of the core. Measured sediment headspace CH_4 values were <0.5 mM in all other cores with the exceptions of PC-07, 14, and 21. In PC-07, 14, and 21, headspace CH_4 concentrations were elevated at depth and increased linearly near the base of each core.

Porewater SO_4^{2-} concentrations in all cores generally decreased with depth from near average seawater values (28.9 mM) at the surface (Figure 3). Most piston cores exhibited a linear decrease in porewater SO_4^{2-} concentrations with depth with clear exceptions being PC-06, 08, and 14. The non-linear porewater SO_4^{2-} profile in PC-06 was consistent with the de-stabilization of solid-phase hydrates. In PC-07, 14, and 21 porewater SO_4^{2-} concentrations decreased to near zero limits of detection and intersected increasing headspace CH_4 values at depth, indicative of an SMT.

Figure 3. Sediment headspace CH_4 and porewater SO_4^{2-} and Cl^- concentrations *vs.* depth (centimeters below sea floor, CMBSF) for AC-07 piston cores (PC). Core PC-06 contained solid phase hydrates which destabilized during collection.

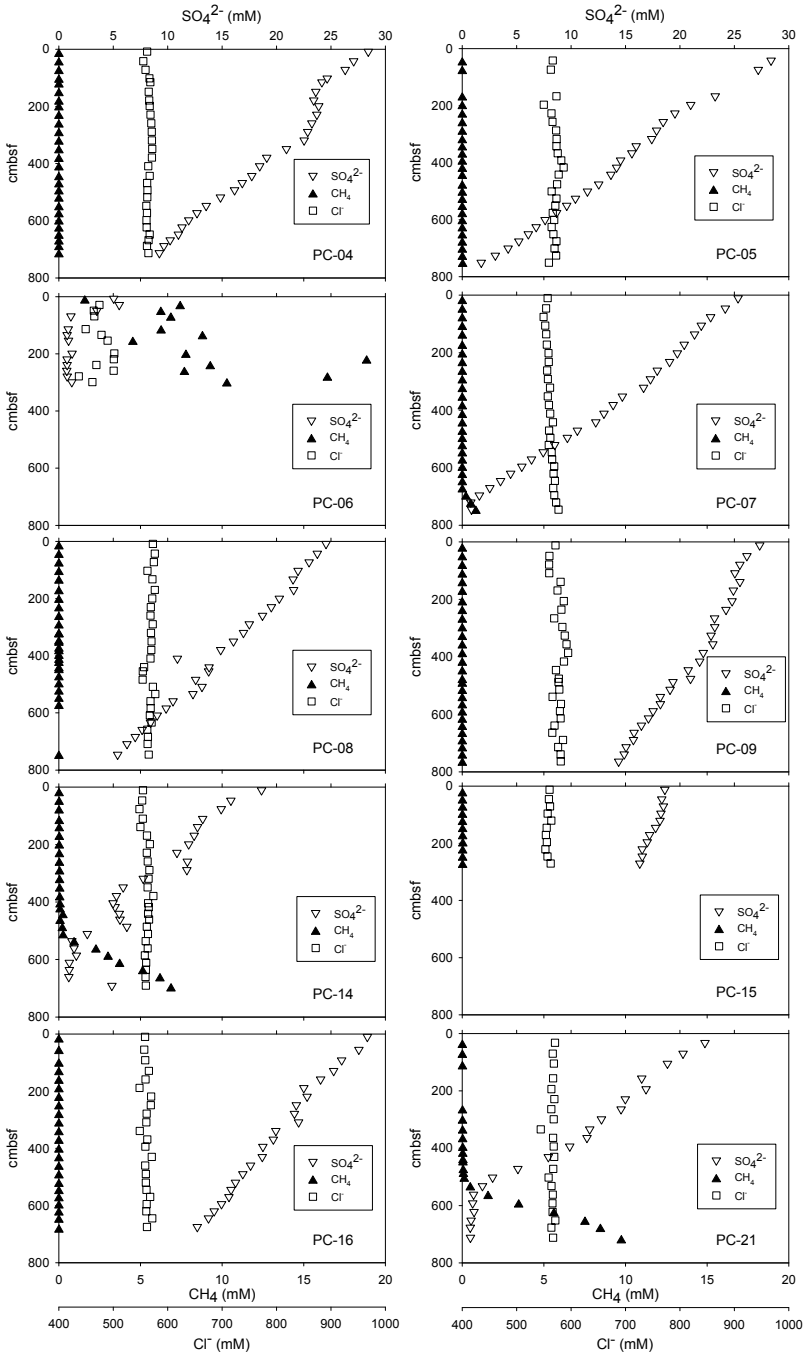

3.2. Porewater Ca^{2+} and Mg^{2+} Concentrations, Ca/Mg Ratios, and Sediment $CaCO_3$ Content

Figure 4 shows measured porewater Ca^{2+} and Mg^{2+} concentrations, Ca/Mg ratios, and estimated sediment $CaCO_3$ content *vs.* depth for AC-07 piston cores. Porewater Ca^{2+} and Mg^{2+} concentrations generally decreased with depth in PC-04, 05, 07, 09, 16, and 21 from near average seawater values of 10.5 mM and 54.1 mM, respectively. The Ca/Mg ratio also decreased with depth in these cores from an average seawater value of ~0.19. Porewater Ca^{2+} and Mg^{2+} concentrations and Ca/Mg ratio profiles showed the most variability with depth in PC-06, 08, 14, and 15. The was no clear trend in estimated

sediment $CaCO_3$ profiles with depth in any of the piston cores collected along AC-07 Inline 986. Estimated sediment $CaCO_3$ content in all cores varied from 5% to 38% by weight.

Figure 4. Porewater Ca^{2+} and Mg^{2+} concentrations, Ca/Mg ratios, and estimated sediment $CaCO_3$ content *vs.* depth (CMBSF) for AC-07 piston cores (PC). Core PC-06 contained solid phase hydrates which destabilized during collection.

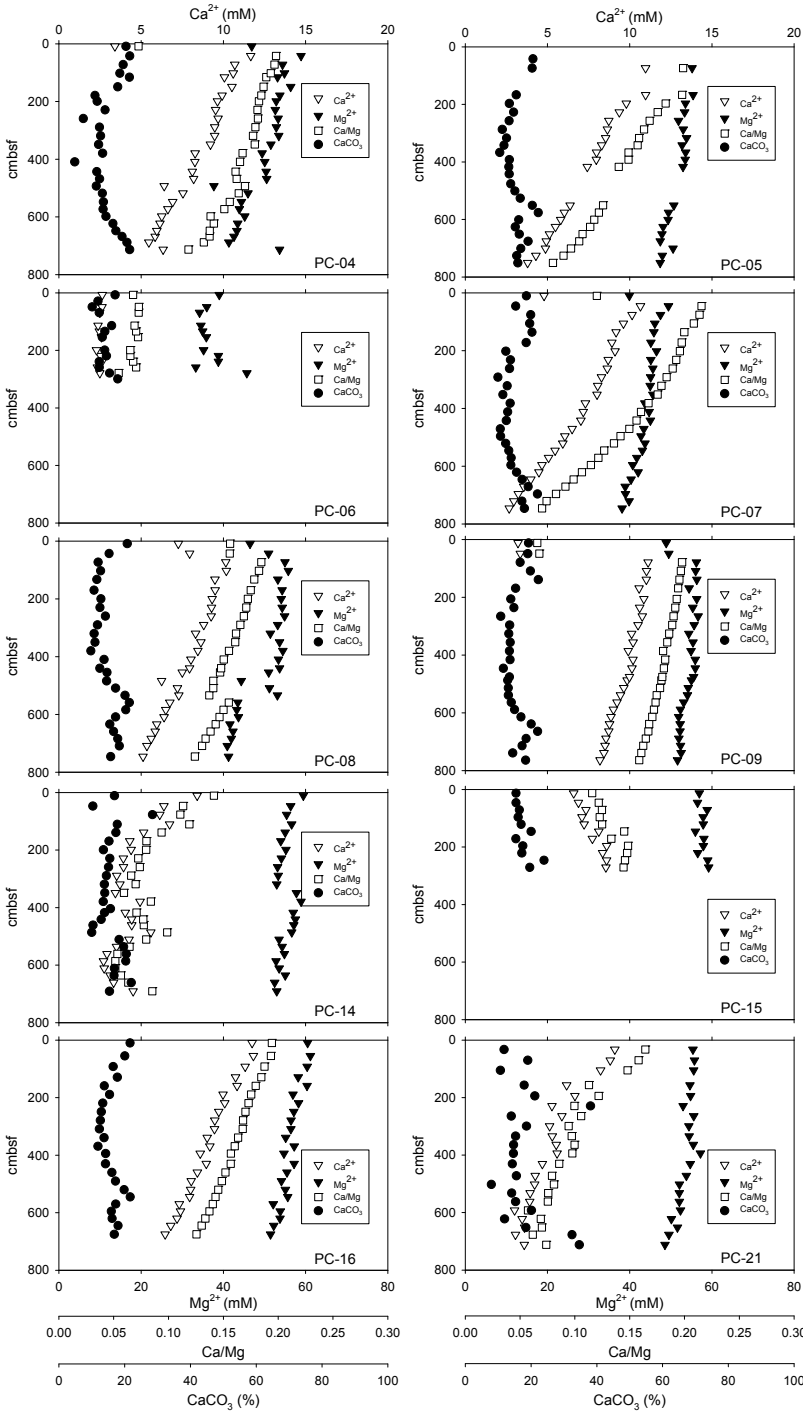

3.3. Porewater DIC Concentrations and δ^{13}C-DIC

Figure 5 shows measured porewater DIC concentrations and DIC stable carbon isotope ratios (δ^{13}C-DIC) *vs.* depth for the AC-07 piston cores. Porewater DIC concentration profiles generally mirrored

porewater SO_4^{2-} concentration profiles (Figure 3), increasing with depth from near average seawater values (2.2 mM) at the surface. In PC-07, 14, 21 porewater DIC concentrations increased with depth to a maximum at the SMT (Figure 3) then decreased below the SMT. As with porewater SO_4^{2-}, Ca^{2+}, Mg^{2+}, and Ca/Mg ratio profiles, most piston cores exhibited a linear trend of increasing porewater DIC concentrations with depth. Most cores, however, showed some non-linearity in porewater DIC profiles. Porewater DIC profiles in PC-06, 08, 09, and 14 exhibited the highest degree of non-linearity. Porewater δ^{13}C-DIC values in the AC-07 cores were closer to average seawater values at the surface (~0‰) becoming more negative, or isotopically-lighter, with depth. In PC-07, 14, and 21 there was a noticeable inflection point in the porewater δ^{13}C-DIC values coincident with the SMT (Figure 3).

Figure 5. Porewater DIC concentrations and DIC stable carbon isotope ratios (δ^{13}C-DIC) *vs.* depth (CMBSF) for AC-07 piston cores (PC). Core PC-06 contained solid phase hydrates which destabilized during collection.

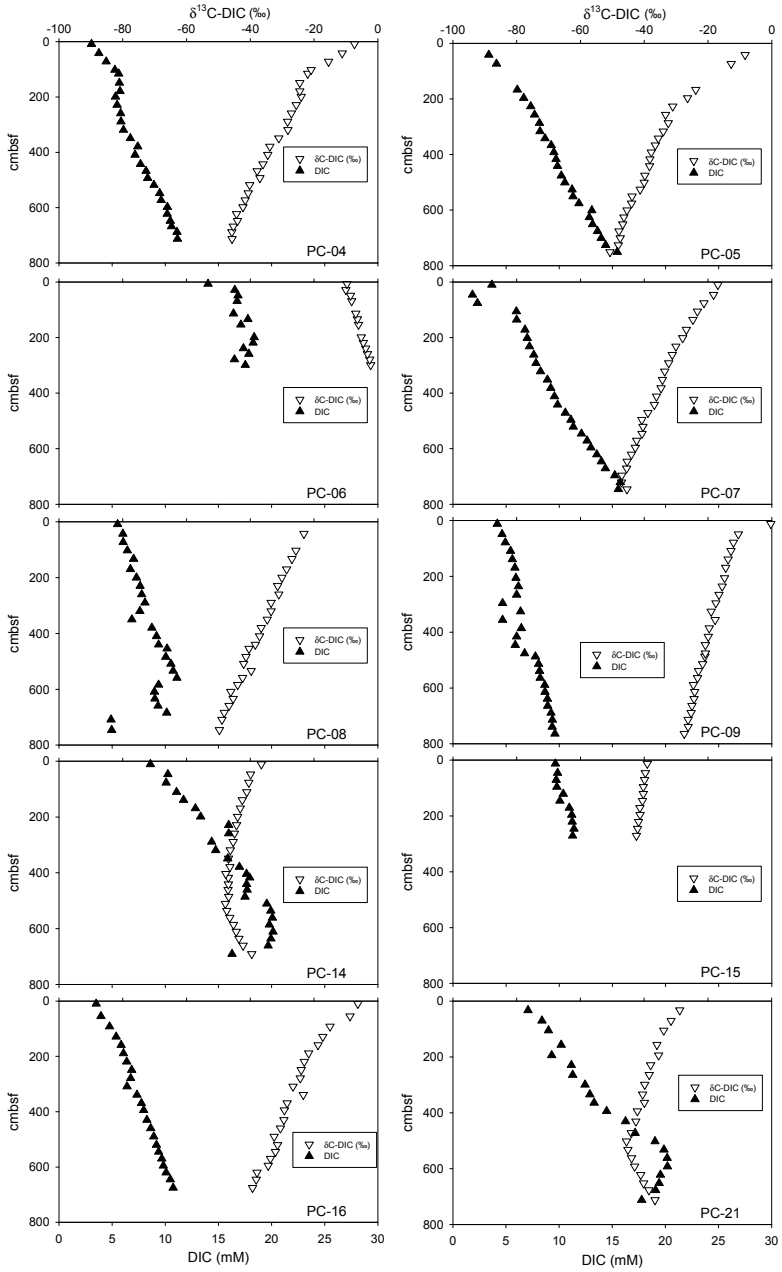

4. Discussion

4.1. Estimated SMT Depths and Sulfate Diffusion Rates

Depths for the sulfate methane transition (SMT) in each core were chosen as the depth where minimum CH_4 and SO_4^{2-} concentrations converge plus half the depth to the next whole round core section. For cores where vertical SO_4^{2-} profiles did not reach the limits of detection, a linear extrapolation of the SO_4^{2-} concentration *vs.* depth profile was used to estimate the depth of the SMT [3,39]. The depth of the SMT provides a relative qualitative prediction of vertical CH_4 flux.

Since porewater CH_4 was not sampled directly, a semi-quantitative, comparative estimate of flux rates between sites was calculated from regression analysis of sediment porewater SO_4^{2-} profiles. A 1:1 ratio of SR to CH_4 oxidation is typically present during AOM [44]. Assuming steady state conditions where AOM is the dominant process consuming sulfate, SO_4^{2-} diffusion rates can be calculated from the linear fit to the SO_4^{2-} concentration gradient according to Fick's first law [45,46]:

$$J = -\varphi \cdot D_s \cdot \frac{dc}{dx} \quad (6)$$

where J represents the SO_4^{2-} flux (mmol/m^2-yr), φ is the sediment porosity, D_s is the diffusion coefficient for sulfate in seawater, c is the range in SO_4^{2-} concentration, and x is the range in depth for the linear section of the SO_4^{2-} porewater profile. D_s in Equation (6) is given by:

$$D_s = \frac{D_0}{1 + n(1 - \varphi)} \quad (7)$$

where D_0 is assumed to be 2.08×10^{-2} m^2/yr, and $n = 3$ for the clay-silt sediments in this region [47]. An average of measured porosity was used in the diffusive flux calculation for each core and, given the shallow cores used in this study, D_0 was assumed to remain constant with depth. As per convention, data presented references downward SO_4^{2-} flux as positive (into the sediments) corresponding to an upward flux (negative) for CH_4 out of the sediments. In sediment cores with non-linear porewater SO_4^{2-} profiles, where possible, the linear portions of the SO_4^{2-} profile below the apparent mixing depth were selected for calculation of the SO_4^{2-} diffusion rate [44–46], otherwise, relative flux between cores was inferred by the depth of the SMT.

In piston cores where SO_4^{2-} profiles were linear, SO_4^{2-} diffusion rates were estimated from the linear fit to the SO_4^{2-} concentration profile, assuming steady state conditions where AOM was the dominant process consuming SO_4^{2-} in a 1:1 ratio to CH_4 [46]. Likewise the depth of the SMT was estimated for cores where the SMT was not present by extrapolating the SO_4^{2-} concentration gradient to a depth where porewater SO_4^{2-} concentrations equaled zero. A similar approach was employed for piston cores with non-linear profiles (AC-06, 08, 14) by using a linear portion of the SO_4^{2-} profile at depth. These results should be viewed as rough relative estimates only since some of these profiles are likely non-steady state (Table 1).

Table 1. Estimated sulfate methane transition (SMT) depths, sulfate diffusion rates ($J_{SO_4^{2-}}$), and average porewater Cl^- concentrations for AC-07 piston cores (PC) referenced to AC-07 PC-08. Core PC-06 contained solid phase hydrates which destabilized during collection.

Core #	AC-07 Core #	Distance from Core #1 (AC-07 PC-08)	Core Length (cm)	SMT (cm)	$J_{SO_4^{2-}}$ (mmol/m^2-yr)	Average Cl^- (mM)	Comments
[1]	08	0.00	759	901	23	568	Non-linear sulfate profile; SMT deeper than max. core depth
[2]	04	0.30	718	1069	21	565	SMT deeper than max. core depth
[3]	07	0.95	759	735	29	562	SMT present
[4]	05	1.70	756	816	26	570	SMT deeper than max. core depth
[5]	06	1.80	309	80	70	468	Non-linear sulfate profile; Solid phase hydrates present, destabilized on recovery
[6]	14	1.83	706	584	28	561	Non-linear sulfate profile; SMT present
[7]	21	1.85	730	585	35	566	SMT present
[8]	15	1.95	284	1278	8	558	SMT deeper than max. core depth
[9]	16	1.98	690	1252	17	561	SMT deeper than max. core depth
[10]	09	2.40	789	1528	13	577	SMT deeper than max. core depth

Figure 6 shows estimated SMT depths, sulfate diffusive flux ($J_{SO_4^{2-}}$), and average porewater Cl^- concentrations (Table 1) over a 3 km linear transect across the suspected seep feature on Inline 986 (Figure 2). The AC-07 cores are referenced to a linear distance from core PC-08. The AC-07 piston cores generally exhibited deep SMTs and low SO_4^{2-} diffusive flux suggesting diffusion-dominated CH_4 flux. Sulfate diffusion rates increased and SMT depths decreased closer to the area on the seafloor where the seismic profiles suggested gas venting and/or the presence of gas hydrates, such as those recovered in PC-06 (Figures 2 and 6). However, in general, the estimated sulfate diffusion rates shown Figure 6 suggest that the shallow sediments of Inline 986 overlay a deep-sea, CH_4 charged sedimentological environment where most, or all, CH_4 diffusing from below is consumed by AOM at the SMT and does not reach the overlying water column [20].

Figure 6. Estimated SMT depths, sulfate diffusion rates ($J_{SO_4^{2-}}$), and average porewater Cl^- concentrations over a 3 km transect across the suspected seep feature shown WesternGeco seismic profile for Inline 986 (Figure 2). Distances are referenced to AC-07 PC-08. Core PC-06 contained solid phase hydrates which destabilized during collection.

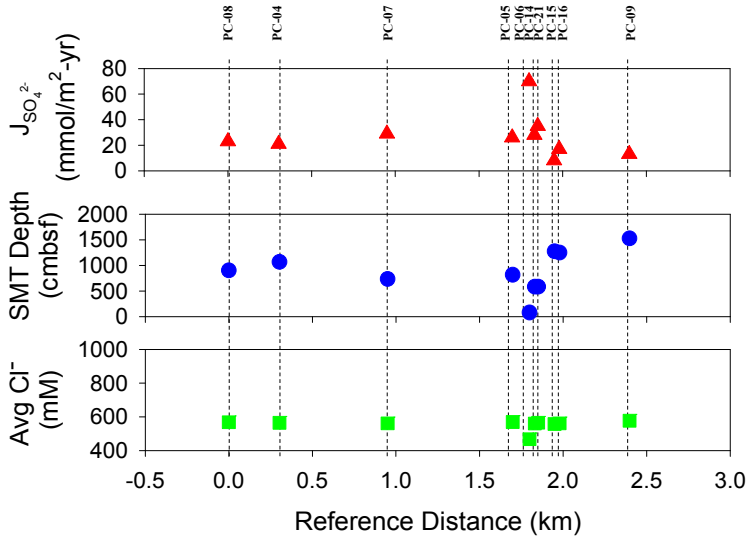

4.2. Diffusive Fluxes of Ca^{2+}, Mg^{2+}, and DIC and Carbon Mass Balance

In sediments where AOM dominates, 1 mole of SO_4^{2-} should be consumed for each mole of CH_4 diffusing upward, producing 1 mole of HCO_3^- (Equation (2)). This is in contrast to organoclastic SR (Equation (1)), where 2 moles of HCO_3^- are produced for each mole of SO_4^{2-} consumed in the breakdown of sediment organic matter. These microbially-mediated processes typically shape the sediment porewater profiles of species like SO_4^{2-} and DIC in organic–rich surface sediments of coastal areas where hydrates are found [21,29,48]. For the AC-07 piston cores in this study which were collected from sediments with a low organic matter content and measurable low vertical CH_4 flux, it is reasonable to assume that AOM is dominating the consumption of SO_4^{2-} and production of HCO_3^- [46]. Seismic data and core porewater data support the assumption of a methane-charged environment. The max sediment organic carbon (SOC) measured in all the piston cores collected was 1.2% organic carbon by weight with an average of only 0.6% organic carbon. Model data from Sivan *et al.* [49] showed that at SOC values <5%, AOM was the dominant microbial process consuming SO_4^{2-} and thus producing HCO_3^- [21].

The over-production of HCO_3^- in porewaters near the SMT due to AOM can lead to the precipitation of authigenic carbonates in the presence of cations like Ca^{2+} and Mg^{2+} via Equation (3) [23]. In theory, if AOM is dominating CH_4 consumption at the SMT in shallow sediments of AC-07 and producing HCO_3^-, then downward diffusion of SO_4^{2-} into sediments ($J_{SO_4^{2-}}$) should be balanced by change in alkalinity due to DIC flux (dominated by HCO_3^-) at a 1:1 ratio [20,21,23,24,29]. However, this simple relation is a gross simplification because of other geochemical process that occur in sediments overlying CH_4-charged deep-sea environments. Over-production of HCO_3^- in porewaters near the SMT due to AOM can lead to precipitation (or dissolution) of authigenic carbonates in the presence of cations like Ca^{2+} and Mg^{2+} changing both alkalinity and DIC concentrations near the SMT [23]. Methanogenesis or thermogenic production of CH_4 occurring below the SMT can also produce an upward DIC flux from below [20,21,23,24,29].

Still, using some simple assumptions, estimates can be made in order to constrain relative CH_4 fluxes and carbon mass balances at sites like AC-07 [20,21,23,24,29]. A net alkalinity flux can be approximated as the net DIC flux [20,21,23,24,29]. The net DIC flux can be approximated as DIC diffusion upward through shallow sediments above the SMT ($J_{\text{DIC-shallow}}$), diffusion of deep DIC upward from below the SMT ($J_{\text{DIC-deep}}$), and loss of DIC to authigenic carbonate phases. Loss of DIC to authigenic carbonate phases ($J_{\text{DIC-carbonate}}$) can be estimated by a loss of major porewater cations like Ca^{2+} and Mg^{2+} as indicated by the downward flux of these cations into sediments from overlying seawater ($J_{Ca^{2+}} + J_{Mg^{2+}}$).

Snyder *et al.* [20] used this method to constrain the mass balance of carbon across the SMT for sediment core from the Umitaka Spur, Japan. In deep-sea, CH_4 charged sedimentological environment like Umitaka Spur and AC-07 where most, or all, CH_4 diffusing from below is consumed by AOM at the SMT and does not reach the overlying water column, then the mass balance of carbon at the SMT can be summarized as:

$$J_{SO_4^{2-}} = -J_{CH_4} = -J_{\text{DIC-net}} = -(J_{\text{DIC-shallow}} - J_{\text{DIC-deep}}) + J_{\text{DIC-carbonate}} \quad (8)$$

The DIC diffusion upward through the shallow sediments above the SMT ($J_{\text{DIC-shallow}}$) and flux of Ca^{2+} and Mg^{2+} into the sediments from the overlying seawater ($J_{Ca^{2+}} + J_{Mg^{2+}}$) can be approximated using the same methods used for $J_{SO_4^{2-}}$ and Equations (6) and (7) assuming a D_0 for HCO_3^-, Ca^{2+}, and Mg^{2+} of 1.94×10^{-2} m^2/yr, 1.36×10^{-2} m^2/yr, and 1.26×10^{-2} m^2/yr, respectively [50]. Given the shallowness of the AC-07 piston cores in relation to the SMT, estimation of the diffusion of DIC upward from below the SMT, or downward to below the SMT, was problematic due to the lack of adequate data points for estimating $J_{\text{DIC-deep}}$. For this study, it is assumed that $J_{\text{DIC-deep}} << J_{\text{DIC-shallow}}$.

Table 2 shows estimated $J_{SO_4^{2-}}$, $J_{\text{DIC-shallow}}$, and $J_{Ca^{2+}}$, $J_{Mg^{2+}}$, and $J_{\text{DIC-net}}$ for the AC-07 piston cores that exhibited (near-) linear profiles of relevant porewater species (SO_4^{2-}, Ca^{2+}, Mg^{2+}, DIC). These cores include PC-04, 05, 09, 16 where the SMT was below the maximum core depth and PC-07 and 21 where the SMT was evident in core porewater profiles. For the AC-07 cores with linear profiles, $J_{SO_4^{2-}} \approx -J_{\text{DIC-shallow}} + J_{\text{DIC-carbonate}}$, where $J_{\text{DIC-carbonate}} = J_{Ca^{2+}} + J_{Mg^{2+}}$.

Table 2. Estimated $J_{SO_4^{2-}}$, $J_{\text{DIC-shallow}}$, and $J_{Ca^{2+}}$, $J_{Mg^{2+}}$, and $J_{\text{DIC-net}}$ for the AC-07 piston cores that exhibited (near-) linear profiles of relevant porewater species (SO_4^{2-}, Ca^{2+}, Mg^{2+}, DIC).

AC-07 Core #	$J_{SO_4^{2-}}$ (mmol/m²-yr)	$J_{\text{DIC-shallow}}$ (mmol/m²-yr)	$J_{Ca^{2+}}$ (mmol/m²-yr)	$J_{Mg^{2+}}$ (mmol/m²-yr)	$J_{\text{DIC-deep}}$ * (mmol/m²-yr)	$J_{\text{DIC-net}}$ (mmol/m²-yr)
04	21	−8	3	8	–	−17
05	26	−11	5	5	–	−21
07	29	−12	7	8	–	−27
09	13	−4	2	3	–	−9
16	17	−7	4	6	–	−17
21	35	−22	4	7	–	−33

* $J_{\text{DIC-deep}}$ not estimated due to the lack of adequate data points.

Estimated values for $J_{SO_4^{2-}}$ plotted against $J_{\text{DIC-net}}$ clearly fall along the 1:1 ratio for AOM (Figure 7). This correlation supports the assumption that AOM is the dominant process consuming SO_4^{2-} in the shallow sediments along AC-07 inline 986. This relationship, however, is a simplification of the actual biogeochemical processes occurring at the SMT in these cores.

Figure 7. Scatter plot of $J_{SO_4^{2-}}$ *vs.* $J_{DIC\text{-}net}$ for the AC-07 piston cores (Table 2). The 1:2 line indicates the molar stoichiometry of SO_4^{2-} consumption to DIC production for organoclastic SR (Equation (1)) and the 1:1 line indicates the molar stoichiometry of SO_4^{2-} consumption to dissolved inorganic carbon production for anaerobic oxidation of methane (Equation (2)).

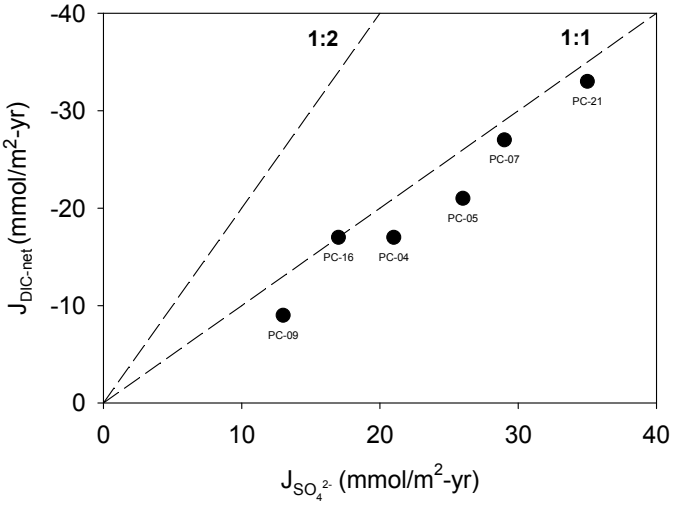

The flux values in Table 2 suggest a large contribution of HCO_3^- to porewaters near the SMT due to AOM. They also suggest that a large portion of this excess DIC is precipitated as authigenic Ca and Mg carbonates. If this is indeed the case then the DIC pool should strongly reflect the isotopic signature of the CH_4 from which is was derived. The contribution of AOM to porewater DIC (HCO_3^-) in each core can be estimated using a mass balance based on the measured δ^{13}C-DIC and δ^{13}C-CH_4 value near the base of cores where the SMT was not present and from the estimated depth of the SMT where it was present [16]:

$$\%DIC_{CH_4} = ((\delta^{13}C\text{-}DIC_{MIN} - \delta^{13}C\text{-}DIC_{SW})/(\delta^{13}C\text{-}CH_{4MIN} - \delta^{13}C\text{-}DIC_{SW})) \times 100 \quad (9)$$

where $\%DIC_{CH4}$ is the contribution of AOM to porewater DIC (HCO_3^-) in each core at or near the SMT, δ^{13}C-DIC_{MIN} is the minimum porewater δ^{13}C-DIC value at or near the SMT, δ^{13}C-DIC_{SW} is the background porewater δ^{13}C-DIC value (assumed for seawater as 0‰), and δ^{13}C-CH_{4MIN} is the minimum measured δ^{13}C-CH_4 value at or near the SMT. Assuming that AOM is the dominant process consuming SO_4^{2-} at the SMT of the AC-07 cores, the percent of the DIC pool that is incorporated into the authigenic carbonate fraction can be estimated as [20]:

$$\%DIC_{carbonate} = (J_{DIC\text{-}carbonate}/J_{SO_4^{2-}}) \times 100 \quad (10)$$

The δ^{13}C-CH_4 values measured at the base of the AC-07 cores or at the SMT ranged from −62‰ to −106‰, suggesting a predominate biogenic source of CH_4 (Table 3). The strongly negative, or isotopically lighter, δ^{13}C-DIC values (−28‰ to −51‰) shown in Table 3 support the assumption that AOM is significantly contributing HCO_3^- to the DIC pool ($\%DIC_{CH_4}$ = 44%–68%) at or near the SMT of each core. Results suggest that a large fraction ($\%DIC_{carbonate}$ = 31% to 59%) of this AOM-derived DIC pool is incorporated into the authigenic carbonate fraction. These estimates are significantly higher than those estimated by others at Umitaka Spur, Japan [20], Hydrate Ridge, and Cascadia Margin [15].

Table 3. Estimates of percent contribution of AOM to the DIC pool and the percent contribution of the DIC pool to solid phase carbonates at the SMT for the AC-07 piston cores (Table 2). The percent contribution of AOM to the DIC pool was based on a mass balance using the minimum measured δ^{13}C-DIC and δ^{13}C-CH_4 value near the base of cores where the SMT was not present and from the estimated depth of the SMT where it was present.

AC-07 Core #	δ^{13}C-DIC_{MIN} (‰)	δ^{13}C-CH_{4MIN} (‰)	$\%DIC_{CH4}$ = %AOM Contribution to the DIC Pool	$\%DIC_{carbonate}$ = %DIC to Carbonate
04	−45.8	−65.7	68	52
05	−50.7	−94.6	54	38
07	−47.1	−105.5	45	52
09	−27.5	−62.5	44	38
16	−39.3	−62.9	62	59
21	−45.5	−93.9	49	31

It is important to note that the flux calculations in Tables 1 and 2, and hence the estimates in Table 3, are based on general assumptions and limited data. The porewater profiles and flux rates used were assumed to be in steady-state. It was assumed that AOM was the dominant process consuming SO_4^{2-} and that no significant amounts of other higher hydrocarbons were present. Presence of higher hydrocarbons, and their subsequent oxidation in porewaters, could result in conditions where $J_{SO_4^{2-}} > -J_{CH_4}$ [30]. Note that even when the DIC flux is corrected to $J_{DIC\text{-}net} = -(J_{DIC\text{-}shallow}) + J_{DIC\text{-}carbonate}$ (Equation (8)) near the SMT for the AC-07 cores, in most cases $J_{SO_4^{2-}} > -J_{DIC\text{-}net}$ (Figure 7). It is also assumed that all CH_4-carbon goes to the DIC pool and is not assimilated into microbial biomass or the organic carbon pool. Previous research by others has shown that <2% of methane-derived carbon is assimilated into biomass [21,51] but some studies suggest that cycling of methane-derived carbon into the organic matter pool may be significant [43]. Other biogeochemical processes like organoclastic SR, fermentation, thermogenic and biogenic methane production, and incorporation of AOM derived HS^- into Fe-sulfide mineral phases can all serve to alter theoretical steady-state porewater profiles for SO_4^{2-} and DIC [20].

Other issues with the flux and budget estimates in this work are that DIC is not a direct measure of HCO_3^- concentration nor does a change in HCO_3^- directly correspond to a change in $CaCO_3$ as shown in Equation (3). In sediments porewaters like those in this work, approximation of total alkalinity to carbonate alkalinity used in deep-ocean waters does not apply. Total alkalinity is a better measure than DIC for changes in porewater chemistry due to HCO_3^- production and carbonate mineralization and precipitation. Changes in the total alkalinity of porewaters can account for changes in major dissolved porewater ions such as Ca^{2+} and Mg^{2+}. Still, if one assumes that changes in porewater alkalinity in methane-charged sediments like those in this study are largely controlled by excess DIC flux dominated by HCO_3^-, then direct measurement of DIC concentrations in porewaters represents an adequate proxy.

Lastly it was assumed that Ca (and Mg) carbonate minerals like calcite and aragonite dominate sediment inorganic carbon in the sediments of AC-07 (Equation (4)). Looking at the Ca^{2+} and Mg^{2+} porewater concentration profiles and the estimated $J_{Ca^{2+}}$ and $J_{Mg^{2+}}$, rates (Table 2) for the AC-07 cores, it is clear that porewater Mg^{2+} concentrations decrease significantly with depth along with Ca^{2+} concentrations. This could be indicative of the formation of dolomite at depth and/or the exchange of

dissolved Mg^{2+} with clays [16,20,52]. Dolomite formation at depth, as demonstrated in studies by others on Blake Ridge [52] and the west African Margin [16], could increase $J_{Mg^{2+}}$, relative to $J_{Ca^{2+}}$, resulting in an overestimation of $J_{DIC\text{-}carbonate}$ and/or a downward flux of DIC below the SMT, thereby impacting $J_{DIC\text{-}deep}$ (not measured in this study). The greater decrease in porewater Ca^{2+} concentrations relative to Mg^{2+} as shown in porewater Ca/Mg ratio profiles in the AC-07 cores (Figure 4), however, is still consistent with the assumption that carbonate formation (calcite and/or aragonite) is the dominant factor controlling $J_{DIC\text{-}carbonate}$.

In summary, the $J_{DIC\text{-}carbonate}$ values (Table 2) and subsequent $\%DIC_{carbonate}$ values (Table 3) in this study likely overestimate the amount of CH_4-derived excess DIC that is precipitated as authigenic Ca and Mg carbonates. A common finding of most biogeochemical studies on carbon cycling in methane charged sediments overlying hydrate bearing strata in areas like Alaminos Canyon is that more data and higher resolution data (with depth) is required to develop an adequate carbon budget [20,21,29]. Still, this study demonstrates that even in low, diffusive dominated flux areas like Alamos Canyon, the incorporation of CH_4-derived excess DIC into authigenic carbonates is significant and simple sediment profiles of SO_4^{2-}, DIC, and other key porewater species provide an adequate first order estimate of CH_4-carbon fluxes and cycling.

5. Conclusions

Results of geochemical characterization of sediments and porewaters collected from the seafloor of the Alaminos Canyon region of the GoM, Inline 986, June 2007 suggest a deep sea, CH_4 charged, diffusion-dominated sedimentological environment where, except in areas of active fluid advection or exposure of solid phase hydrate near the seafloor (PC-06), most of the CH_4 diffusing up through the sediments from the GHSZ below is consumed by AOM at the SMT. Estimated SO_4^{2-} diffusion rates ($J_{SO_4^{2-}}$) ranged from 8 to 70 mmol/m^2-yr. A simple stable isotope mass balance using the minimum measured $\delta^{13}C$-DIC and $\delta^{13}C$-CH_4 values near the base of the AC-07 cores and/or SMT supports the assumption that AOM is significantly contributing HCO_3^- to the DIC pool ($\%DIC_{CH_4}$ = 44%–68%) at or near the SMT. When DIC flux is corrected to $J_{DIC\text{-}net}$ to account for the incorporation of CH_4-AOM-derived DIC into solid phase carbonates, the resulting stoichiometric balance of 1:1 for $J_{SO_4^{2-}}$:$J_{DIC\text{-}net}$ supports the assumption of an AOM dominated system.

Although this study likely overestimates the incorporation of CH_4-derived excess DIC into authigenic carbonates, results support the conclusion that incorporation of CH_4-derived carbon into dissolved and solid inorganic carbon phases represents a significant carbon sink and plays a role in regulating the flux of methane to the overlying water column and atmosphere at Alaminos Canyon and potentially other site with CH_4 hydrate bearing marine sediments. More data and better sampling resolution is required for detailed assessments of carbon cycling in CH_4-charged sediments but sediment profiles of SO_4^{2-}, DIC, and other key porewater species used in this study provide an adequate, first-order estimate of CH_4-carbon fluxes and cycling in Alaminos Canyon.

Acknowledgments

This work was supported, in part, through a National Research Council (NRC) Postdoctoral Research Associateship sponsored by the U.S. Naval Research Laboratory (NRL), Marine Biogeochemistry

Section (Code 6114). This study was conducted as part of the NRL Seep and Methane Hydrate Advanced Research Initiative (ARI) model development in collaboration with the U.S. Department of Energy, National Energy Technology Laboratory (NETL). Fieldwork planning integrated a preliminary geochemical survey for the Gulf of Mexico Gas Hydrate Joint Industry Project (JIP) drilling on Alaminos Canyon, Block 818 and locations for field sampling and data collection were based on seismic profiles provide by WesternGeco after review by WesternGeco, NRL, NETL and Mineral Management Service (MMS). Special thanks to the AC-07 research team and their collaborators and the Captain and crew of the R/V Cape Hatteras.

Author Contributions

This work was a collaborative research effort between the two authors, Joseph P. Smith and Richard B. Coffin. The first author was the primary author in the writing of the specific research focus of this paper.

Conflicts of Interest

The authors declare no conflict of interest.

References

1. Kvenvolden, K.A.; Lorenson, T.D. The global occurrence of natural gas hydrate. *Am. Geophys. Union* **2001**, *124*, 3–18.
2. Borowski, W.S.; Paull, C.K.; Ussler, W., III. Global and local variations of interstitial sulfate gradients in deep-water, continental margin sediments: Sensitivity to underlying methane and gas hydrates. *Mar. Geol.* **1999**, *159*, 131–154.
3. Coffin, R.B.; Hamdan, L.; Plummer, R.; Smith, J.P.; Gardner, J.; Hagen, R.; Wood, W. Analysis of methane and sulfate flux in methane-charged sediments from the Mississippi Canyon, Gulf of Mexico. *Mar. Pet. Geol.* **2008**, *25*, 977–987.
4. Hutchinson, D.R.; Hart, P.E.; Ruppel, C.D.; Snyder, F.; Dugan, B. Seismic and thermal Characterization of a Bottom Simulating Reflection in the Northern Gulf of Mexico. In *Natural Gas Hydrates: Energy Resources, Potential and Associated Geologic Hazards*; Collett, T.S., Johnson, A., Knapp, C., Boswell, R., Eds.; AAPG Special Publication Memoir: Tulsa, OK, USA, 2009; Volume 89, pp. 266–286.
5. Charlou, J.L.; Donval, J.P.; Fouquet, Y.; Ondreas, H.; Knoery, J.; Cochonat, P.; Levaché, D.; Poirier, Y.; Jean-Baptiste, P.; Fourré, E.; *et al.* Physical and chemical characterization of gas hydrates and associated methane plumes in the Congo-Angola basin. *Chem. Geol.* **2004**, *205*, 405–425.
6. Sassen, R.; Roberts, H.H.; Carney, R.; Milkov, A.V.; Freitas, D.A.; Lanoil, B.; Zhang, C. Free hydrocarbon gas, gas hydrate, and authigenic minerals in chemosynthetic communities of northern Gulf of Mexico continental slope: Relation to microbial processes. *Chem. Geol.* **2004**, *205*, 195–217.
7. Paull, C.K.; Matsumoto, R.; Wallace, P.J.; Dillon, W.P. *Proceedings of the Ocean Drilling Program: Initial Reports*; Ocean Drilling Program: College Station, TX, USA, 1996; Volume 164.

8. Xu, W.Y.; Ruppel, C. Predicting the occurrence, distribution, and evolution of methane gas hydrate in porous marine sediments. *J. Geophys. Res.* **1999**, *104*, 5081–5096.
9. Cooper, A.K.; Hart, P.E. High-resolution seismic-reflection investigation of the northern Gulf of Mexico gas hydrate stability zone. *Mar. Pet. Geol.* **2003**, *19*, 1275–1293.
10. Bohrmann, G.; Greinert, J.; Suess, E.; Torres, M. Authigenic carbonates from the Cascadia subduction zone and their relation to gas hydrate stability. *Geology* **1998**, *26*, 647–650.
11. Aloisi, G.; Pierre, C.; Rouchy, J.-M.; Foucher, J.-P.; Woodside, J. Methane-related authigenic carbonates of eastern Mediterranean Sea mud volcanoes and their possible relation to gas hydrate destabilisation. *Earth Planet. Sci. Lett.* **2000**, *184*, 321–338.
12. Naehr, T.H.; Rodriguez, N.M.; Bohrmann, G.; Paull, C.K.; Botz, R. Methane-derived authigenic carbonates associated with gas-hydrate decomposition and fluid venting above the blake ridge diapir. In *Proceedings of the Ocean Drilling Program: Science Results*; Paull, C.K., Matsumoto, R., Wallace, P.J., Dillon, W.P., Eds.; Ocean Drilling Program: College Station, TX, USA, 2000; Volume 164, pp. 285–295.
13. Rodriguez, N.M.; Paull, C.K.; Borowski, W.S. Zonation of authigenic carbonates within gas hydrate-bearing sedimentary sections on the blake ridge: offshore southeastern North America. In *Proceedings of the Ocean Drilling Program: Science Results*; Paull, C.K., Matsumoto, R., Wallace, P.J., Dillon, W.P., Eds.; Ocean Drilling Program: College Station, TX, USA, 2000; Volume 164, pp. 301–312.
14. Greinert, J.; Bohrmann, G.; Suess, E. Gas hydrate associated carbonates and methane-venting at hydrate ridge: classification, distribution and origin of authigenic lithologies. In *Natural Gas Hydrates: Occurrence, Distribution, and Detection*; Paull, C.K., Dillon, W.P., Eds.; AGU Geophysical Monograph, American Geophysical Union: Washington, DC, USA, 2001; Volume 124, pp. 99–113.
15. Luff, R.; Wallmann, K. Fluid flow, methane fluxes, carbonate precipitation and biogeochemical turnover in gas hydrate-bearing sediments at hydrate ridge, Cascadia margin: Numerical modeling and mass balances. *Geochim. Cosmochim. Acta* **2003**, *67*, 3403–3421.
16. Moore, T.S.; Murray, R.W.; Kurtz, A.C.; Schrag, D.P. Anaerobic methane oxidation and the formation of dolomite. *Earth Planet. Sci. Lett.* **2004**, *229*, 141–154.
17. Formolo, M.J.; Lyons, T.W.; Zhang, C.; Kelley, C.; Sassen, R.; Horita, J.; Cole, D.R. Quantifying carbon sources in the formation of authigenic carbonates at gas hydrate sites in the Gulf of Mexico. *Chem. Geol.* **2004**, *205*, 253–264.
18. Mazzini, A.; Ivanov, M.K.; Parnell, J.; Stadnitskaia, A.; Cronin, B.T.; Poludetkinab, E.; Mazurenko, L.; van Weering, T.C.E. Methane-related authigenic carbonates from the Black Sea: Geochemical characterisation and relation to seeping fluids. *Mar. Geol.* **2004**, *212*, 153–181.
19. Berelson, W.M.; Prokopenko, M.; Sansone, F.J.; Graham, A.W.; McManus, J.; Bernhard, J.M. Anaerobic diagenesis of silica and carbon in continental margin sediments; discrete zones of TCO_2 production. *Geochim. Cosmochim. Acta* **2005**, *69*, 4611–4629.
20. Snyder, G.T.; Hirutab, A.; Matsumoto, R.; Dickens, G.R.; Tomaru, H.; Takeuchi, R.; Komatsubara, J.; Ishida, Y.; Yua, H. Pore water profiles and authigenic mineralization in shallow marine sediments above the methane-charged system on Umitaka Spur, Japan Sea. *Deep Sea Res. II* **2007**, *54*, 1216–1239.

21. Ussler, W., III; Paull, C.K. Rates of anaerobic oxidation of methane and authigenic carbonate mineralization in methane-rich deep-sea sediments inferred from models and geochemical profiles. *Earth Planet. Sci. Lett.* **2008**, *266*, 271–287.
22. Boetius, A.; Suess, E. Hydrate Ridge: A natural laboratory for the study of microbial life fueled by methane from near-surface gas hydrates. *Chem. Geol.* **2004**, *205*, 291–310.
23. Kastner, M.; Elderfield, H.; Martin, J.B.; Suess, E.; Kvenvolden, K.A.; Garrison, R.E. Diagenesis and interstitial-water chemistry at the peruvian continental margin-major constituents and strontium isotopes. In *Proceedings of the Ocean Drilling Program: Science Results*; Suess, E., von Huene, R., Emeis, K.-C., Bourgois, J., Castaneda, J.C., de Wever, P., Eglinton, G., Garrison, R., Greenberg, M., Paz, E.H., *et al.*; Eds.; Ocean Drilling Program: College Station, TX, USA, 1990; Volume 112, pp. 413–440.
24. Chatterjee, S.; Dickens, G.R.; Bhatnagar, G.; Chapman, W.G.; Dugan, B.; Snyder, G.T.; Hirasaki, G.J. Pore water sulfate, alkalinity, and carbon isotope profiles in shallow sediment above marine gas hydrate systems: A numerical modeling perspective. *J. Geophys. Res.* **2011**, doi:10.1029/2011JB008290.
25. Valentine, D.L. Biogeochemistry and microbial ecology of methane oxidation in anoxic environments: A review. *Antonie Van Leeuwenhoek* **2002**, *81*, 271–282.
26. Bayon, G.; Pierre, C.; Henderson, G.M.; Etoubleau, J.; Voisset, M.; Canquil, E.; Fouquet, Y. Sr/Ca and Ma/Ca ratios in sediments from the Niger fan: Evidence for past episodes of gas hydrate dissociation. *Geophys. Res. Abstr.* **2005**, *7*, 08714:1–08714:2.
27. Burton, E.A. Controls on marine carbonate cement mineralogy: Review and assessment. *Chem. Geol.* **1993**, *105*, 291–310.
28. Paull, C.K.; Ussler, W.; Lorenson, T.D.; Winters, W.; Dougherty, J.A. Geochemical constraints on the distribution of gas hydrates in the Gulf of Mexico. *Geo-Mar. Lett.* **2005**, *25*, 273–280.
29. Dickens, G.R.; Snyder, G.T. Interpreting upward methane flux from marine pore water profiles. In *Fire in the Ice*; National Energy Technology Laboratory, U.S. Department of Energy: Washington, DC, USA, 2009; pp. 7–10.
30. Joye, S.B.; Boetius, A.; Orcutt, B.N.; Montoya, J.P.; Schulz, H.N.; Erickson, M.J.; Lugo, S.K. The anaerobic oxidation of methane and sulfate reduction in sediments from Gulf of Mexico cold seeps. *Chem. Geol.* **2004**, *205*, 219–238.
31. Kvenvolden, K.A. Gas hydrates-geological perspective and global change. *Rev. Geophys.* **1993**, *31*, 173–187.
32. Sloan, E.D. *Clathrate Hydrates of Natural Gasses*, 2nd ed.; Marcel Dekker, Inc.: New York, NY, USA, 1998; p. 705.
33. Trudgill, B.; Rowan, M.; Fiduk, J.; Weimer, P.; Gale, P.; Korn, B.; Phair, R.; Gafford, W.; Roberts, G.; Dobbs, S. The Perdido Fold Belt, northwestern Gulf of Mexico, Part 1: Structural geology, evolution, and regional implications. *Am. Assoc. Pet. Geol. Bull.* **1999**, *83*, 88–113.
34. Boswell, R.; Shelander, D.; Lee, M.; Latham, T.; Collett, T.; Guerin, G.; Moridis, G.; Reagan, M.; Goldberg, D. Occurrence of gas hydrate in Oligocene Frio sand: Alaminos Canyon Block 818: Northern Gulf of Mexico. *Mar. Pet. Geol.* **2009**, *26*, 1499–1512.

35. Fiduk, J.; Weimer, P.; Trudgill, B.; Rowan, M.; Gale, P.; Phair, R.; Korn, B.; Roberts, G.; Gafford, W.; Lowe, R.; *et al.* The Perdido Fold Belt, northwestern Gulf of Mexico, Part 2: Seismic stratigraphy and petroleum systems. *Am. Assoc. Pet. Geol. Bull.* **1999**, *83*, 578–612.
36. Meyer, D.; Zarra, L.; Rains, D.; Meltz, B.; Hall, T. Emergence of the lower Tertiary Wilcox trend in the deepwater Gulf of Mexico. *World Oil* **2005**, *226*, 72–77.
37. Cordes, E.; Carney, S.; Hourdez, S.; Carney, R.; Brooks, J.; Fisher, C. Cold seeps of the deep Gulf of Mexico: Community structure and biogeographic comparisons to Atlantic equatorial belt seep communities. *Deep Sea Res. 1 Oceanogr. Res. Pap.* **2007**, *54*, 637–653.
38. Roberts, H.; Fisher, C.; Brooks, J.; Bernard, B.; Carney, R.; Cordes, E.; Shedd, W.; Hunt, J.; Joye, S.; MacDonald, I.; *et al.* Exploration of the deep gulf of mexico slope using dsv alvin: site selection and geologic character. In Proceedings of the 57th Annual Convention of the Gulf Coast Association of Geological Societies (GCAGS), Corpus Christi, TX, USA, 21–23 October 2007.
39. Coffin, R.B.; Hamdan, L.J.; Smith, J.P.; Rose, K.; Downer, R.; Edsall, D.; Gardner, J.; Hagen, R.; Wood, W. *Geochemical Evaluation of Deep Sediment Hydrate Deposits on Alaminos Canyon, Block 818, Texas-Louisiana Shelf*; Cruise Report for UNOLS Ship R/V CAPE HATTERAS Cruise NRL AC-07, U.S. Naval Research Laboratory: Washington, DC, USA, 2008; p. 173.
40. Hoehler, T.M.; Borowski, W.S.; Alperin, M.J.; Rodriguez, N.M.; Paull, C.K. Model stable isotope and radiocarbon characterization of anaerobic methane oxidation in gas hydrate-bearing sediments of the blake ridge. In *Proceedings of the Ocean Drilling Program: Science Results*; Paull, C.K., Matsumoto, R., Wallace, P.J., Dillon, W.P., Eds.; Ocean Drilling Program: College Station, TX, USA, 2000; Volume 164, pp. 79–85.
41. Boehme, S.E.; Blair, N.E.; Chanton, J.P.; Martens, C.S. A mass balance of ^{13}C and ^{12}C in an organic-rich methane-producing marine sediment. *Geochim. Cosmochim. Acta* **1996**, *60*, 3835–3848.
42. Plummer, R.E.; Pohlman, J.W.; Coffin, R.B. Compound-specific stable carbon isotope analysis of low-concentration complex hydrocarbon mixtures from natural gas hydrate systems. In Proceedings of the EOS American Geophysical Union (AGU) Fall Meeting Supplement, San Francisco, CA, USA, 5–9 December 2005; Volume 86.
43. Coffin, R.B.; Hamdan, L.; Smith, J.P.; Rose, P.S.; Plummer, R.E.; Yoza, B.A.; Pecher, I.; Montgomery, M.T. The contribution of vertical methane flux to shallow sediment carbon pools across the Porangahau Ridge, New Zealand. *Energies* **2014**, *7*, 5332–5356.
44. Borowski, W.S.; Paull, C.K.; Ussler, W., III. Marine porewater sulfate profiles indicate *in situ* methane flux from underlying gas hydrate. *Geology* **1996**, *24*, 655–658.
45. Berner, R.A. An idealized model of dissolved sulfate distribution in recent sediments. *Geochim. Cosmochim. Acta* **1964**, *28*, 1497–1503.
46. Berner, R.A. Sulfate reduction and the rate of deposition of marine sediments. *Earth Planet. Sci. Lett.* **1978**, *37*, 492–498.
47. Iversen, N.; Jørgensen, B.B. Diffusion coefficients of sulfate and methane in marine sediments: Influence of porosity. *Geochim. Cosmochim. Acta* **1992**, *57*, 571–578.
48. Kastner, M.; Torres, M.; Solomon, E.; Spivack, A.J. Marine pore fluid profiles of dissolved sulfate: Do they reflect *in situ* methane fluxes? In *Fire in the Ice*; National Energy Technology Laboratory, U.S. Department of Energy: Washington, DC, USA, 2008; pp. 6–8.

49. Sivan, O.; Schrag, D.P.; Murray, R.W. Rates of methanogenesis and methanotrophy in deep-sea sediments. *Geobiology* **2007**, *5*, 141–151.
50. Atkins, P.W. *Physical Chemistry*; Oxford University Press: Oxford, UK, 1978; p. 1022.
51. Nauhaus, K.; Albrecht, M.; Elvert, M.; Boetius, A.; Widdel, F. *In vitro* cell growth of marine archaeal-bacterial consortia during anaerobic oxidation of methane with sulfate. *Environ. Microbiol.* **2007**, *9*, 187–196.
52. Cağatay, M.N.; Borowski, W.S.; Ternois, Y.G. Factors affecting the diagenesis of Quaternary sediments at ODP Leg 172 sites in western north Atlantic. *Chem. Geol.* **2001**, *175*, 467–484.

© 2014 by the authors; licensee MDPI, Basel, Switzerland. This article is an open access article distributed under the terms and conditions of the Creative Commons Attribution license (http://creativecommons.org/licenses/by/3.0/).